Dopant incorporation in $Al_{0.9}Ga_{0.1}As_{0.06}Sb_{0.94}$ grown by molecular beam epitaxy

Saroj Kumar Patra[1, §], Thanh-Nam Tran[1], Lasse Vines[2], Ilia Kolevatov[2], Edouard Monakhov[2] and Bjørn-Ove Fimland[1, §§]

[1] Department of Electronics and Telecommunications,

Norwegian University of Science and Technology (NTNU), NO-7491 Trondheim, Norway

[2]Department of Physics,

University of Oslo, NO-0316 Oslo, Norway

§Electronic mail: saroj.kumar.patra@ntnu.no
§§Electronic mail: bjorn.fimland@ntnu.no

Abstract

Incorporation of beryllium (Be) and tellurium (Te) dopants in epitaxially grown $Al_{0.9}Ga_{0.1}As_{0.06}Sb_{0.94}$ layers was investigated. Carrier concentrations and mobilities of the doped layers were obtained from room temperature Hall effect measurements, and dopant densities from secondary ion mass spectrometry depth profiling. An undoped $Al_{0.3}Ga_{0.7}As$ cap layer and side wall passivation were used to reduce oxidation and improve accuracy in Hall effect measurements. The measurements on Be-doped samples revealed high doping efficiency and the carrier concentration varied linearly with dopant density up to the highest Be-dopant density of 2.9×10^{19} cm^{-3}, whereas for Te-doped samples the doping efficiency was in general low and the carrier concentration saturated for Te-dopant densities above 8.0×10^{18} cm^{-3}. The low doping efficiency in Te-doped $Al_{0.9}Ga_{0.1}As_{0.06}Sb_{0.94}$ layer was studied by deep-

1

level transient spectroscopy, revealing existence of deep trap levels and related DX-centers which explains the low doping efficiency.

1. Introduction

Mid-infrared lasers emitting in the 2-3 μm wavelength range are very important for trace gas sensing using tunable diode-laser absorption spectroscopy (TDLAS) [1]. GaSb-based III-V semiconductor quantum well diode lasers cover this particular wavelength range. CH_4 has a very strong absorption line at 2.3 μm wavelength [2-4], and therefore GaInAsSb/AlGaAsSb-based lasers emitting at that particular wavelength are of high interest [5-8]. For such diode lasers, $Al_{0.9}Ga_{0.1}As_ySb_{1-y}$ lattice-matched to GaSb is used as cladding layers [5, 9-12]. Lattice-matching at growth temperature, i.e. $Al_{0.9}Ga_{0.1}As_{0.06}Sb_{0.94}$, is preferred to have dislocation free layers [9]. Te and Be are used as n-type dopant and p-type dopant, respectively, in the cladding layers [10, 13-15]. Characteristics of these diode lasers are dependent on parameters used during growth of laser materials and fabrication of diode lasers. For example, composition, thickness and strain in the quantum wells and barriers affect the emission wavelength of the diode laser [2]. The resistance and threshold current density of the diode depend strongly on the carrier concentration in the cladding layers and the thickness of the

2

undoped core. Increase in resistance gives rise to heating, which leads to increase in Auger loss [16] and thus reduction in laser output power. Therefore, the output power of the laser depends on the doping in the cladding layers. Optimization of the output power of the diode laser requires calibrations of incorporated dopant density and corresponding carrier concentration in the cladding layers. However, there has been limited work reported on the dopant incorporation in AlGaAsSb [17, 18].

In this paper, we present new data on carrier concentration versus dopant incorporation in $Al_{0.9}Ga_{0.1}As_{0.06}Sb_{0.94}$ layers grown by molecular beam epitaxy (MBE). A number of Be- and Te-doped $Al_{0.9}Ga_{0.1}As_{0.06}Sb_{0.94}$ layers were grown on undoped GaAs(001) substrates, using different Be and GaTe source temperatures. A 100 nm thick undoped $Al_{0.3}Ga_{0.7}As$ cap layer was grown on top of the doped $Al_{0.9}Ga_{0.1}As_{0.06}Sb_{0.94}$ layer to reduce oxidation and errors in Hall effect measurements. Carrier concentrations and Hall mobilities of the doped $Al_{0.9}Ga_{0.1}As_{0.06}Sb_{0.94}$ layers were obtained from room temperature Hall effect measurements for different Be- and Te-dopant densities, as measured by secondary ion mass spectrometry (SIMS) depth profiling. Deep-level transient spectroscopy (DLTS) was performed on $Al_{0.9}Ga_{0.1}As_{0.06}Sb_{0.94}$/GaSb diodes to study the low doping efficiency in Te-doped cladding layers. The low doping efficiency can be explained by the existence of acceptor-like DX-centers due to deep level defects.

2. Experimental

2.1. Material growth

Two different types of test structures were grown in a Varian GEN II Modular MBE system equipped with Te and Be dopant furnaces, an Al dual crucible furnace, a Ga dual filament furnace, and Veeco As and Sb valved cracker furnaces. GaTe and Be sources were outgassed

for 30 minutes at a temperature 20 ^{0}C higher than the maximum used temperature and stabilized at the required temperature prior to growth.

The first type of test structures, for Hall effect and SIMS measurements, were grown at 520 ^{0}C on epi-ready undoped GaAs(001) 2" quarter wafers. Prior to growth, native oxide was desorbed at 585 ^{0}C followed by wafer annealing at 610 ^{0}C for 15 minutes under an As$_2$ pressure of 1.0×10^{-6} Torr. 2 μm thick doped Al$_{0.9}$Ga$_{0.1}$As$_{0.06}$Sb$_{0.94}$ layer followed by a 100 nm thick undoped Al$_{0.3}$Ga$_{0.7}$As cap layer were grown at 1 ML/sec growth rate. Al$_{0.3}$Ga$_{0.7}$As was chosen as the cap layer in order to prevent both oxidation of the doped Al$_{0.9}$Ga$_{0.1}$As$_{0.06}$Sb$_{0.94}$ layer as well as formation of a conducting 2-dimensional sheet at the interface between the doped Al$_{0.9}$Ga$_{0.1}$As$_{0.06}$Sb$_{0.94}$ layer and the undoped cap layer. Al$_{0.3}$Ga$_{0.7}$As has an appropriate band gap and band gap alignment with respect to the doped Al$_{0.9}$Ga$_{0.1}$As$_{0.06}$Sb$_{0.94}$ layer for our experiment. Ten Be-doped Al$_{0.9}$Ga$_{0.1}$As$_{0.06}$Sb$_{0.94}$ samples with different Be source temperature (925 ^{0}C to 1150 ^{0}C) and seven Te-doped Al$_{0.9}$Ga$_{0.1}$As$_{0.06}$Sb$_{0.94}$ samples with different GaTe source temperature (415 ^{0}C to 495 ^{0}C) were grown.

The second type of test structures, for DLTS measurements, were grown at 520 ^{0}C on epi-ready n-type (Te) doped GaSb(001) 2" quarter wafers. Native oxide desorption and wafer annealing prior to growth were performed at 550 ^{0}C under an Sb$_2$ pressure of 1.3×10^{-6} Torr. 1 μm thick Te-doped Al$_{0.9}$Ga$_{0.1}$As$_{0.06}$Sb$_{0.94}$ layer followed by a 100 nm thick Be-doped GaSb layer were grown at a growth rate of 1 ML/sec. Three samples with different Te-doping in the Al$_{0.9}$Ga$_{0.1}$As$_{0.06}$Sb$_{0.94}$ layer and fixed Be-doping in the GaSb layer were grown as summarized in Table 1.

Table 1: Be-doped GaSb/Te-doped $Al_{0.9}Ga_{0.1}As_{0.06}Sb_{0.94}$ PN-diode samples for DLTS measurements. Listed dopant densities are based on experimental SIMS data.

Sample ID	Be dopant density in GaSb (cm^{-3})	Te dopant density in $Al_{0.9}Ga_{0.1}As_{0.06}Sb_{0.9}$ (cm^{-3})
Sb 284	5.0×10^{18}	3.0×10^{18}
Sb 285	5.0×10^{18}	2.0×10^{18}
Sb 286	5.0×10^{18}	1.0×10^{18}

2.2. Device fabrication

Hall bar samples with six-contact 1-2-2-1 geometry were fabricated from the first type of test structures. Pattern for six metal contact pads were created by conventional photolithography using the photoresist ma-N 440. Prior to metallization, the surface oxide layer was removed by wet chemical etching using $NH_4OH:H_2O_2:H_2O$ (1:1:200) for 30 seconds and $NH_4OH: H_2O$ (1:30) for 1 minute. 1.5 μm thick Au layer was deposited using an e-beam metal deposition system followed by a metal lift-off in acetone for ~10 minutes to define the contact pads. The Hall bar was defined by a second photolithography process followed by a wet chemical etching with etch depth of 3 μm using citric acid (2.5M):H_2O_2:H_2O (1:1:20) for 90 seconds. To prevent oxidation of the sidewall of Hall bar samples, photoresist ma-N 440 was used as passivation layer. Rapid thermal annealing (RTA) of the Au contacts at 400 ^{0}C for 20 seconds lead to the diffusion of Au through the $Al_{0.3}Ga_{0.7}As$ cap layer, as confirmed from energy-dispersive x-ray (EDX) analysis (micrographs not shown), and formed ohmic contact to the doped $Al_{0.9}Ga_{0.1}As_{0.06}Sb_{0.94}$ layer. The final contacts to the Hall bar samples were formed by wire bonding to a printed circuit board using Au wire.

Be-doped GaSb/ Te-doped $Al_{0.9}Ga_{0.1}As_{0.06}Sb_{0.94}$ PN junction diodes were fabricated from the second type of test structures for DLTS measurements. 800 μm × 800 μm patterns for metal contact pads were created on the front side (i.e. Be-doped GaSb) of the sample using

conventional photolithography. Prior to metallization, GaSb surface oxide was removed *in situ* by Ar sputtering at 325 eV in a combined sputtering and e-beam evaporation system (AJA ATC-2200V) [19]. A Ti/Pt/Au (50 nm/25 nm/325 nm) metal stack was deposited using e-beam metal deposition followed by a metal lift-off by acetone to define front contact pads. Using a photoresist mask, covering the front contact pads, the diode structures were defined by dry etching using BCl_3 to an etch depth of 3 μm (i.e. etching into the Te-doped GaSb substrate). A sidewall-passivation layer was formed using photoresist to prevent surface oxidation. A Pd/Ge/Au/Pt/Au (8.7 nm/56 nm/23.3 nm/47.6 nm/200 nm) metal stack [20, 21] was deposited on the back side of the sample to form an ohmic bottom contact. The metal contacts were annealed at 290 ^{0}C for 45 seconds using RTA.

2.3. Characterization

Carrier concentration and Hall mobility for the doped $Al_{0.9}Ga_{0.1}As_{0.06}Sb_{0.94}$ samples were measured using a Lakeshore 7504 Hall effect electronic transport measurement system. Room temperature Hall effect measurements were performed with varying magnetic field from 0 T to 0.5 T in both directions.

SIMS measurements were employed using a Cameca IMS7f microanalyzer. Depth profiles for Te-doped $Al_{0.9}Ga_{0.1}As_{0.06}Sb_{0.94}$ samples were obtained using 15 keV Cs^+ ions as primary beam; depth profiles for Be-doped $Al_{0.9}Ga_{0.1}As_{0.06}Sb_{0.94}$ samples were obtained using 10 keV O_2^+ ions as primary beam. For Cs^+ primary beam, ^{27}Al, ^{69}Ga, ^{75}As, ^{121}Sb and ^{128}Te of the secondary species were monitored. ^{128}Te was used since it appeared to have the least interferences with respect to species/molecules with similar mass, or mass to charge ratio, based on mass spectra taken from different samples. For O_2^+ primary beam, ^9Be, ^{75}As and $^{71}Ga_2$ were monitored. The $^{71}Ga_2$ molecule was used to monitor the matrix as the signal from single ^{71}Ga was too strong. Crater depths were measured with a Dektak 8 stylus profilometer,

and a constant erosion rate was assumed when converting sputtering time to sample depth. From measuring the depths of several craters, an average sputter rate of 2.1 nm/second was found for both of the primary beams, and this sputter rate is assumed for all presented depth profiles for Be and Te. Concentration calibrations were performed using an ^{56}Fe implanted reference sample. The reference sample had the same epilayer structure as the other doped samples, except that an undoped $Al_{0.9}Ga_{0.1}As_{0.06}Sb_{0.94}$ layer was grown instead of a Be- or Te-doped $Al_{0.9}Ga_{0.1}As_{0.06}Sb_{0.94}$ layer. The SIMS intensity (counts/s) to concentration (cm^{-3}) calibrations were performed by measuring the implanted profile with the same SIMS parameters before and after the measurements of the doped samples. The relative sensitivity factor (RSF) for the Te calibration was 2.2×10^{15} and that for the Be calibration was 1.0×10^{14}.

The DLTS measurements were performed in the temperature range of 30 K - 300 K with a reverse bias voltage of -1 V and –0.5 V, and a pulse voltage of 1 V and 0.5 V (50 ms duration) using a refined version of the setup described elsewhere [22]. The DLTS signal was extracted applying a lock-in weighting function with different rate windows in the range (20 ms)$^{-1}$ to (640 ms)$^{-1}$.

3. Results and discussions

Carrier concentration and Hall mobility values from Hall effect measurements and average dopant density values from SIMS measurements for Be-doped $Al_{0.9}Ga_{0.1}As_{0.06}Sb_{0.94}$ samples and for Te-doped $Al_{0.9}Ga_{0.1}As_{0.06}Sb_{0.94}$ samples are summarized in Table 2 and in Table 3, respectively.

Table 2: Be-doped $Al_{0.9}Ga_{0.1}As_{0.06}Sb_{0.94}$ samples: Carrier concentration and Hall mobility values from Hall effect measurements and average dopant density values from SIMS measurements.

| Sample ID	Be source temperature (^{0}C)	Carrier concentration (cm^{-3})	Hall mobility ($cm^{2}/V.s$)	Average dopant density (cm^{-3})
As 642	925	5.5×10^{16}	111	1.0×10^{17}
As 641	950	1.2×10^{17}	122	2.2×10^{17}
As 640	975	3.2×10^{17}	107	4.1×10^{17}
As 634	1000	7.2×10^{17}	102	8.4×10^{17}
As 635	1025	1.4×10^{18}	88	1.6×10^{18}
As 636	1050	3.0×10^{18}	74	2.9×10^{18}
As 637	1075	6.1×10^{18}	61	5.1×10^{18}
As 638	1100	1.2×10^{19}	51	9.6×10^{18}
As 639	1125	2.2×10^{19}	45	1.8×10^{19}
As 644	1150	3.7×10^{19}	42	2.9×10^{19}

Table 3: Te-doped $Al_{0.9}Ga_{0.1}As_{0.06}Sb_{0.94}$ samples: Carrier concentration and Hall mobility values from Hall effect measurements and average dopant density values from SIMS measurements.

Sample ID	GaTe source temperature (^0C)	Carrier concentration (cm^{-3})	Hall mobility ($cm^2/V.s$)	Average dopant density (cm^{-3})
As 606-1	415	$< 1.0 \times 10^{17}$	-	3.7×10^{17}
As 608-4	430	1.1×10^{17}	41	5.7×10^{17}
As 602-2	450	1.3×10^{17}	30	2.3×10^{18}
As 608-3	465	1.6×10^{17}	24	8.3×10^{18}
As 606-2	475	1.6×10^{17}	20	1.4×10^{19}
As 606-4	485	1.6×10^{17}	19	2.4×10^{19}
As 606-3	495	1.6×10^{17}	21	3.8×10^{19}

The change in average dopant density in Be-doped $Al_{0.9}Ga_{0.1}As_{0.06}Sb_{0.94}$ with temperature of the Be source is presented in figure 1. The average dopant density was determined from the SIMS depth profile by finding the average of dopant density values in the 200-2000 nm depth range. The exponential fit to the data is in conformity with the conventional Arrhenius behavior. Variations of carrier concentration and Hall mobility with average dopant density for Be-doped $Al_{0.9}Ga_{0.1}As_{0.06}Sb_{0.94}$ samples are shown in figure 2. The carrier concentration varies linearly with Be-dopant density and does not saturate up to the Be density of 2.9×10^{19} cm^{-3}. As expected, the Hall mobility for holes decreases with increasing Be dopant density and is in general lower as compared to that of p-type GaAs [23] and p-type GaSb [24].
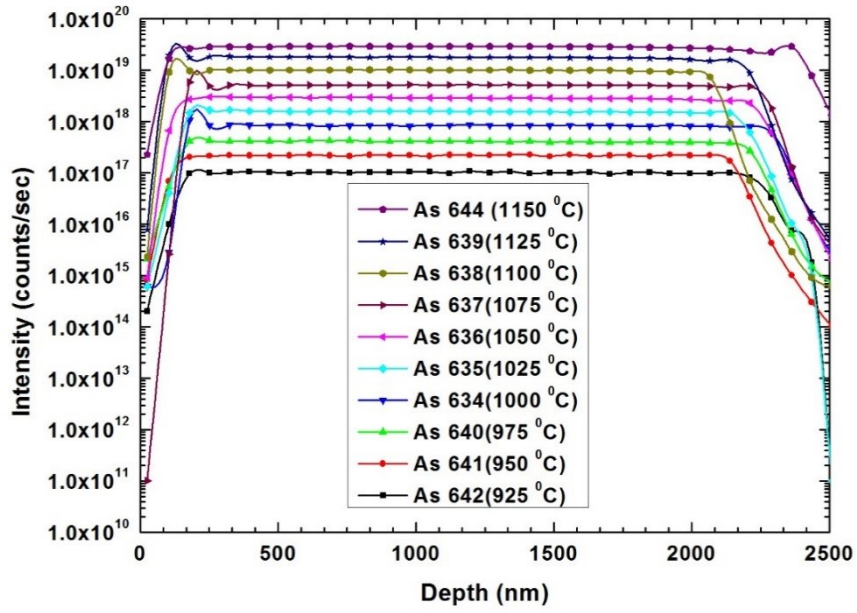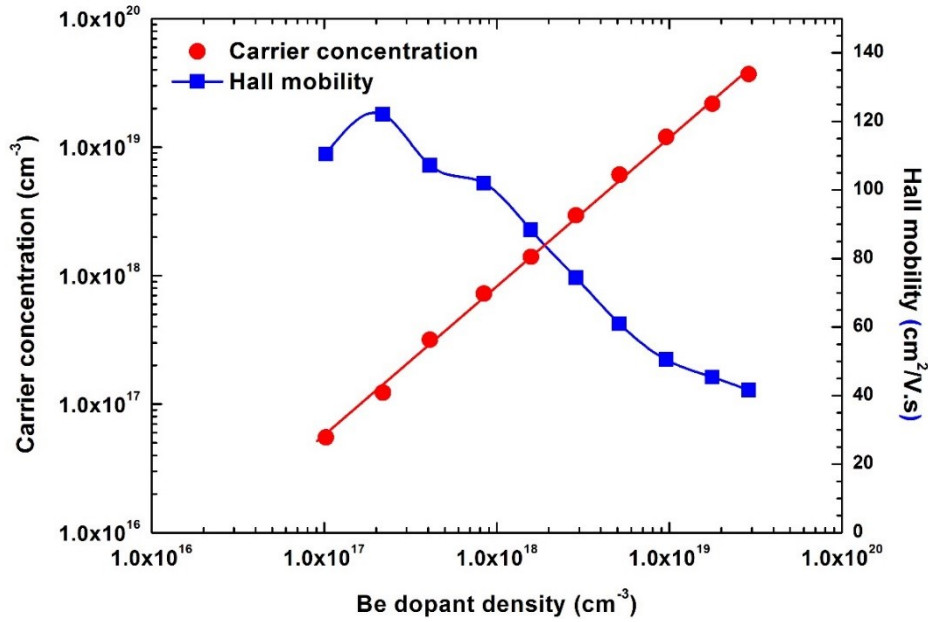
(a)
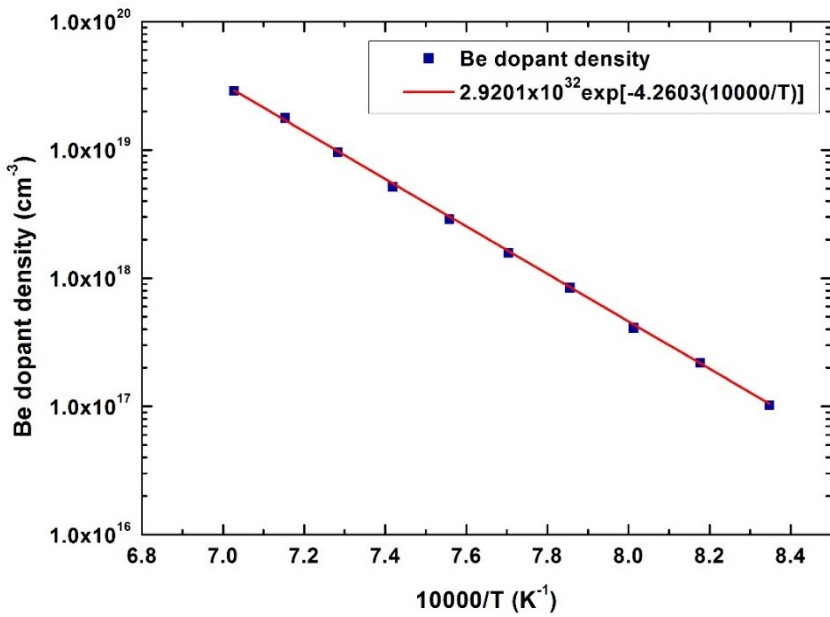
(b)

Figure 1 (color online): Variation in Be dopant density in $Al_{0.9}Ga_{0.1}As_{0.06}Sb_{0.94}$ with temperature of the Be source. (a) SIMS depth profile in Be-doped $Al_{0.9}Ga_{0.1}As_{0.06}Sb_{0.94}$ samples with undoped $Al_{0.3}Ga_{0.7}As$ cap layer. (b) Variation in Be dopant density in $Al_{0.9}Ga_{0.1}As_{0.06}Sb_{0.94}$ with inverse of absolute temperature (T) of the Be source.
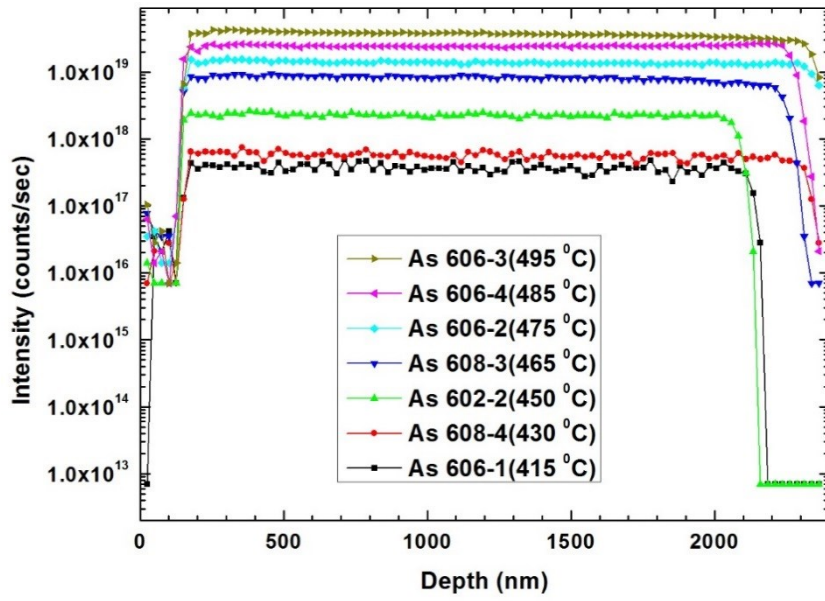
Figure 2 (color online): Variation in carrier concentration and Hall mobility with Be dopant density in Be-doped Al$_{0.9}$Ga$_{0.1}$As$_{0.06}$Sb$_{0.94}$. Drawn lines are guides to the eye only.

Due to a lattice mismatch of 7.96%, the Al$_{0.9}$Ga$_{0.1}$As$_{0.06}$Sb$_{0.94}$ epilayer grown on the GaAs(001) substrate is compressively strained and will start relaxing beyond its critical thickness of a few monolayers. We expect this to leave an array of periodic dislocations at the interface, similar to what is shown for AlSb grown on GaAs(001) substrate [25] (8.54% lattice mismatch) and for GaSb grown on GaAs(001) substrate [26] (7.85% lattice mismatch). However, Vaughan et al. [25] reported that the threading dislocation density for AlSb epilayer grown on GaAs(001), albeit large near the interface, reduces significantly as the AlSb growth progresses. Raisin et al. [26] found that after 25 nm of GaSb growth on GaAs, 99% of the lattice mismatch strain had relaxed. They explained the low density of threading defects in the GaSb epilayer (at least two orders of magnitude smaller at the level of the interface than in the 4.09% mismatched GaAs/Si system) as being due to the high quality of misfit dislocation network in the GaSb/GaAs system. Likewise, there will be defects at the interface between the Al$_{0.9}$Ga$_{0.1}$As$_{0.06}$Sb$_{0.94}$ epilayer and the Al$_{0.3}$Ga$_{0.7}$As cap layer, as the latter will relax due to

tensile strain. Carrier concentration and mobility are in general sensitive to growth conditions, defects and impurity levels. In our case, the favorable band bending near the interfaces between the doped $Al_{0.9}Ga_{0.1}As_{0.06}Sb_{0.94}$ and the undoped GaAs and $Al_{0.3}Ga_{0.7}As$ should reduce the interaction between the majority carriers and the defects. The linear variation of hole concentration versus Be dopant density shown in figure 2 also indicates that the interaction between majority carriers and defects does not dramatically affect the carrier concentration. We should here also mention that Bennett et al. [27] found that the doping efficiencies of Be in GaAs on undoped GaAs(001) substrate and AlSb on undoped GaAs(001) substrate were equal in the 10^{16} – 10^{19} cm^{-3} range (using 5 nm undoped GaSb cap on the doped AlSb epilayer), consistent with previous measurement results in our group [28].

The change in average dopant density in Te-doped $Al_{0.9}Ga_{0.1}As_{0.06}Sb_{0.94}$ with temperature of the GaTe source is presented in figure 3. The average dopant density was determined from the SIMS depth profile by finding the average of dopant density values in the 200-2000 nm range. The variations of free carrier concentration and Hall mobility with average dopant density for Te-doped $Al_{0.9}Ga_{0.1}As_{0.06}Sb_{0.94}$ samples are shown in figure 4. The free carrier concentration saturates at 1.6×10^{17} cm^{-3} for Te dopant density 8.0×10^{18} cm^{-3} and hence the doping efficiency is only 2% at dopant density of 8.0×10^{18} cm^{-3}. Due to saturation in carrier concentration, addition of dopants beyond 8.0×10^{18} cm^{-3} only creates more defects as the dopants possibly stay at the interstitial sites in the crystal structure or/and form complexes. Possibly, annealing at a temperature higher than the growth temperature could enhance the doping efficiency and hence increase carrier concentration [29]. However, Te-doped $Al_{0.9}Ga_{0.1}As_{0.06}Sb_{0.94}$ is used as the cladding layer in mid-infrared lasers and annealing of lasers at high temperature is not preferred to avoid interdiffusion effects in the quantum wells and barriers and hence change in emitted wavelength [30, 31].
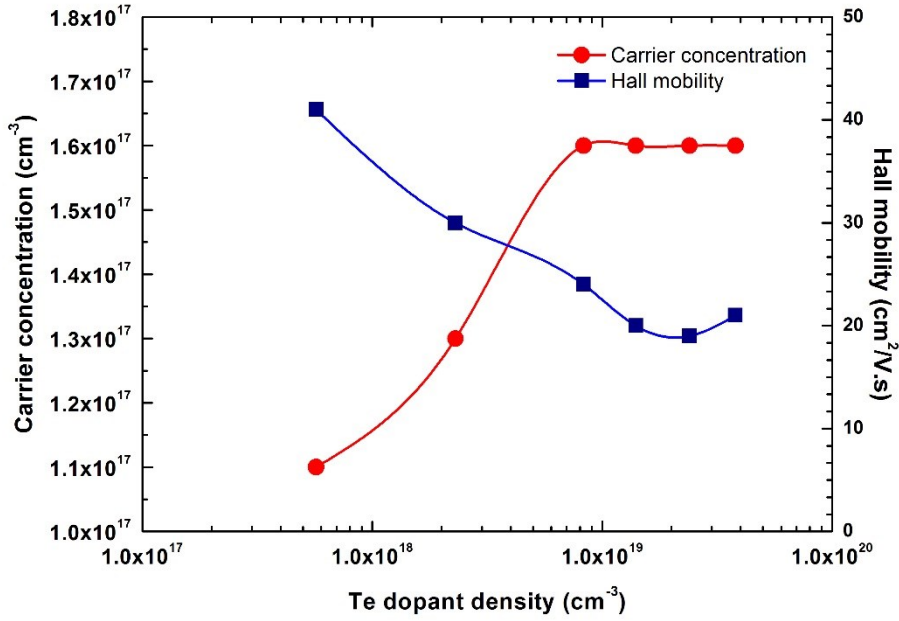
(a)
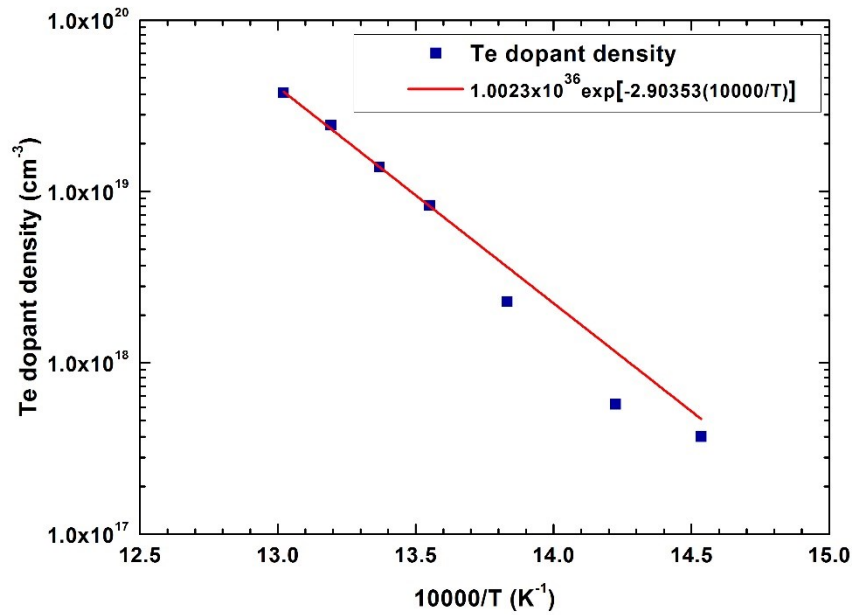
(b)

Figure 3 (color online): Te dopant density in $Al_{0.9}Ga_{0.1}As_{0.06}Sb_{0.94}$ versus temperature of the GaTe source. (a) SIMS depth profile in Te-doped $Al_{0.9}Ga_{0.1}As_{0.06}Sb_{0.94}$ samples with undoped $Al_{0.3}Ga_{0.7}As$ cap layer. (b) Variation in Te dopant density in $Al_{0.9}Ga_{0.1}As_{0.06}Sb_{0.94}$ with inverse of absolute temperature (T) of the GaTe source.

Figure 4 (color online): Variation in carrier concentration and Hall mobility with Te dopant density in Te-doped Al$_{0.9}$Ga$_{0.1}$As$_{0.06}$Sb$_{0.94}$. Drawn lines are guides to the eye only.

Chiu et al. [32] found from Hall effect measurements on 2 μm thick Te-doped GaSb epilayers on undoped GaAs(001) substrates that, for growth temperatures below 540 ^{0}C, the free carrier concentration was very close to the Te dopant concentration (determined from SIMS) for Te concentrations in the 1×10^{17} cm^{-3} to 1×10^{18} cm^{-3} range. This shows that the dislocation and threading defects in the GaSb/GaAs system do not significantly affect the doping efficiency of Te in the GaSb epilayer in this range and we expect the same to be the case for our Te-doped Al$_{0.9}$Ga$_{0.1}$As$_{0.06}$Sb$_{0.94}$ samples. Chiu et al. [32] also found that the free carrier concentration saturates at around 1.5×10^{18} cm^{-3} for Te dopant density around 2-3 $\times$ 10^{18} cm^{-3} and that the free carrier concentration decreases for higher Te dopant densities. These findings are consistent with previous measurement results in our group [28] where we found the free carrier concentration to saturate at 1.8×10^{18} cm^{-3}.

The low doping efficiency effects in Te-doped $Al_{0.9}Ga_{0.1}As_{0.06}Sb_{0.94}$ are further investigated by DLTS measurements. DLTS signals for three Be-doped GaSb/ Te-doped $Al_{0.9}Ga_{0.1}As_{0.06}Sb_{0.94}$ PN diode samples with rate window $(640\ ms)^{-1}$ are shown in figure 5. $\Delta C/C$ represents the ratio of trap concentration to total dopant concentration [33]. Two dominant deep level defects are observed in all the samples: a shallower level with a peak DLTS signature around 120 K and a deeper level around 220 K. However, the peak temperature of both defects levels vary between samples. This may indicate that (i) the origin of the observed defects levels are not the same in Sb 284 – Sb 286; (ii) the observed defects are donors and the emissions rates are influences by Poole-Frenkel effect [34]; (iii) the tunneling leakage is high enough to affect the DLTS signatures of the observed defects [35]. Hence, further investigations are needed to elucidate the origin of the defect levels. The high concentration of the electrically active centers in the Sb 284 sample also demonstrates that they have a strong impact on the carrier concentration, and may partially explain the reduced dopant activation in these samples.

According to Bourgoin et al. [36], the donor impurities in III-V semiconductors introduce two states, viz. a shallow state associated with the Γ-band and a deep state associated with the L-band and hence the introduction of DX-centers. Nakagawa et al. [37] have reported the presence of deep DX-center-like electron traps in AlSb. According to Baraldi et al. [38], these DX-centers have deep energy levels below the conduction band absolute minimum. The density of DX-centers depends exponentially on the energy difference between the Fermi energy (E_F) and the energy of the DX-center (E_{DX}) and the carrier concentration decreases with an increase in density of these DX-centers. Therefore, low doping efficiency in Te-doped $Al_{0.9}Ga_{0.1}As_{0.06}Sb_{0.94}$ is most likely due to presence of DX-centers.
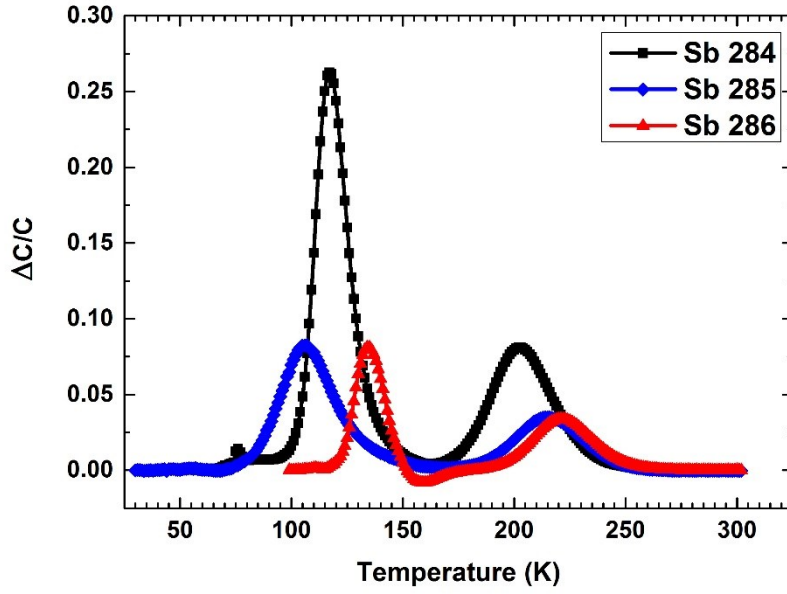
Figure 5 (color online): DLTS signal for three Be-doped GaSb/Te-doped $Al_{0.9}Ga_{0.1}As_{0.06}Sb_{0.94}$ PN-diode samples with rate window $(640\ ms)^{-1}$. Te dopant densities were 3.0×10^{18} cm^{-3} (Sb 284), 2.0×10^{18} cm^{-3} (Sb 285) and 1.0×10^{18} cm^{-3} (Sb 286).

4. Conclusions

In this work, dependence of carrier concentration and Hall mobility on dopant density for both Be- and Te-doped $Al_{0.9}Ga_{0.1}As_{0.06}Sb_{0.94}$ was investigated. Use of undoped $Al_{0.3}Ga_{0.7}As$ cap layer and photoresist passivation layer helped in reducing oxidation and hence improving accuracy in measurements for carrier concentration and Hall mobility. Carrier concentration was found to vary linearly with dopant density for Be-doped $Al_{0.9}Ga_{0.1}As_{0.06}Sb_{0.94}$, whereas it saturates at 8.0×10^{18} cm^{-3} dopant density for Te-doped $Al_{0.9}Ga_{0.1}As_{0.06}Sb_{0.94}$. As per DLTS measurements, low doping efficiency in Te-doped $Al_{0.9}Ga_{0.1}As_{0.06}Sb_{0.94}$ is due to presence of deep trap levels.

ACKNOWLEDGMENTS

REFERENCES

[1] L.S. Rothman, D. Jacquemart, A. Barbe, D. Chris Benner, M. Birk, L. Brown, M. Carleer, C. Chackerian Jr, K. Chance, L. Coudert, et al., The *HITRAN* 2004 molecular spectroscopic database, Journal of Quantitative Spectroscopy and Radiative Transfer, **96** (2005) 139-204. `DOI:10.1016/j.jqsrt.2004.10.008`

[2] E. Tournié, A.N. Baranov, Mid-Infrared Semiconductor Lasers: A Review, in: J. J. Coleman, B. Catrina, C. Jagadish (Eds.) Advances in Semiconductor Lasers, Academic Press, 2012, pp. 183-226. `ISBN:9780123910660`

[3] S. Lundqvist, P. Kluczynski, Process analytical applications in the Mid-Infrared, Quantum Sensing and Nanophotonic Devices VIII, Proc SPIE, **7945** (2011) 79450N. `DOI:10.1117/12.871571`

[4] M. Jahjah, S. Moumdji, O. Gauthier-Lafaye, S. Bonnefont, Y. Rouillard, A. Vicet, Antimonide-based 2.3 μm photonic crystal coupled-cavity lasers for CH_4, Electronics Letters, **48** (2012) 277 - 278. `DOI:10.1049/el.2011.3614`

[5] D. Donetsky, G. Kipshidze, L. Shterengas, T. Hosoda, G. Belenky, 2.3 μm type-I quantum well GaInAsSb/AlGaAsSb/GaSb laser diodes with quasi-cw output power of 1.4 W, Electronics Letters, **43** (2007) 810-812. `DOI:10.1049/el:20071320`

[6] D.Z. Garbuzov, H. Lee, V. Khalfin, R. Martinelli, J.C. Connolly, G.L. Belenky, 2.3-2.7-μm room temperature CW operation of InGaAsSb-AlGaAsSb broad waveguide SCH-QW diode lasers, Photonics Technology Letters, IEEE, **11** (1999) 794-796. `DOI:10.1109/68.769710`

[7] A. Vicet, J.C. Nicolas, F. Genty, Y. Rouillard, E.M. Skouri, A.N. Baranov, C. Alibert, Room temperature GaInAsSb/GaSb quantum well laser for tunable diode laser absorption spectroscopy around 2.35 μm, IEE Proceedings - Optoelectronics, **147** (2000) 172-176. `DOI:10.1049/ip-opt:20000298`

[8] Y. Rouillard, J. Angellier, A. Salhi, P. Grech, F. Chevrier, GaInAsSb/AlGaAsSb laser diodes for the 2- to 3-μm range, Novel In-Plane Semiconductor Lasers XI, Proc. SPIE, **5738** (2005) 120-129. `DOI:10.1117/12.597118`

[9] M. Breivik, T.A. Nilsen, G. Myrvågnes, E. Selvig, B.-O. Fimland, Temperature dependent lattice constant of $Al_{0.9}Ga_{0.1}As_ySb_{1-y}$, Journal of Vacuum Science & Technology B, **28** (2010) C3I1-C3I5. `DOI:10.1116/1.3414830`

[10] A. Gassenq, L. Cerutti, A.N. Baranov, E. Tournié, MBE growth of mid-IR diode lasers based on InAs/GaSb/InSb short-period superlattice active zones, Journal of Crystal Growth, **311** (2009) 1905-1907. `DOI:10.1016/j.jcrysgro.2008.10.074`

[11] G.W. Turner, H.K. Choi, M.J. Manfra, Ultralow-threshold (50 A/cm^2) strained single-quantum-well GaInAsSb/AlGaAsSb lasers emitting at 2.05 μm, Applied Physics Letters, **72** (1998) 876-878. `DOI:10.1063/1.120922`

[12] J.N. Walpole, H.K. Choi, L.G. Missaggia, Z.L. Liau, M.K. Connors, G.W. Turner, M.J. Manfra, C.C. Cook, High-power high-brightness GaInAsSb-AlGaAsSb tapered laser arrays with anamorphic collimating lenses emitting at 2.05 μm, Photonics Technology Letters, IEEE, **11** (1999) 1223-1225. `DOI:10.1109/68.789698`

[13] J.A. Gupta, P.J. Barrios, J. Lapointe, G.C. Aers, C. Storey, Single-mode 2.4 μm InGaAsSb/AlGaAsSb distributed feedback lasers for gas sensing, Applied Physics Letters, **95** (2009) 041104. DOI:10.1063/1.3189814

[14] G.W. Turner, H.K. Choi, D.R. Calawa, J.V. Pantano, J.W. Chludzinski, Molecular-beam epitaxy growth of high-performance midinfrared diode lasers, Journal of Vacuum Science & Technology B, **12** (1994) 1266-1268. DOI:10.1116/1.587018

[15] S.J. Eglash, H.K. Choi, G.W. Turner, MBE growth of GaInAsSb/AlGaAsSb double heterostructures for infrared diode lasers, Journal of Crystal Growth, **111** (1991) 669-676. DOI:10.1016/0022-0248(91)91061-E

[16] R.G. Bedford, G. Triplett, D.H. Tomich, S.W. Koch, J. Moloney, J. Hader, Reduced auger recombination in mid-infrared semiconductor lasers, Journal of Applied Physics, **110** (2011) 073108-073106. DOI:10.1063/1.3646552

[17] A.Z. Li, J.X. Wang, Y.L. Zheng, G.P. Ru, W.G. Bi, Z.X. Chen, N.C. Zhu, The behavior of dopant incorporation and internal strain in $Al_xGa_{1-x}As_{0.03}Sb_{0.97}$ grown by molecular beam epitaxy, Journal of Crystal Growth, **127** (1993) 566-569. DOI:10.1016/0022-0248(93)90684-O

[18] H. Ehsani, N. Lewis, G.J. Nichols, L. Danielson, M.W. Dashiell, Z.A. Shellenbarger, C.A. Wang, Effect of substrate surface defects and Te dopant concentration on crystalline quality and electrical characteristics of AlGaAsSb epitaxial layers, Journal of Crystal Growth, **291** (2006) 77-81. DOI:10.1016/j.jcrysgro.2006.02.054

[19] T.-N. Tran, S.K. Patra, M. Breivik, B.-O. Fimland, Plasma-assisted oxide removal from p-type GaSb for low resistivity ohmic contacts, Journal of Vacuum Science & Technology B, **33** (2015) 061210. DOI:10.1116/1.4935883

[20] N. Rahimi, A.A. Aragon, O.S. Romero, D.M. Kim, N.B.J. Traynor, T.J. Rotter, G. Balakrishnan, S.D. Mukherjee, L.F. Lester, Ohmic contacts to n-type GaSb grown on GaAs by the interfacial misfit dislocation technique, Physics, Simulation, and Photonic Engineering of Photovoltaic Devices II, Proc SPIE, **8620** (2013) 86201K. DOI:10.1117/12.2003392

[21] A. Vogt, A. Simon, H. Hartnagel, J. Schikora, V. Buschmann, M. Rodewald, H. Fuess, S. Fascko, C. Koerdt, H. Kurz, Ohmic contact formation mechanism of the PdGeAu system on n-type GaSb grown by molecular beam epitaxy, Journal of Applied Physics, **83** (1998) 7715-7719. DOI:10.1063/1.367943

[22] B.G. Svensson, K.H. Rydén, B.M.S. Lewerentz, Overlapping electron traps in n-type silicon studied by capacitance transient spectroscopy, Journal of Applied Physics, **66** (1989) 1699-1704. DOI:10.1063/1.344389

[23] B.G. Streetman, S. Banerjee, Solid state electronic devices, 6th ed., Prentice-Hall, New Jersey, 2005. ISBN:9780131497269

[24] J.D. Wiley, Chapter 2 Mobility of Holes in III-V Compounds, in: R.K. Willardson, C.B. Albert (Eds.) Semiconductors and Semimetals, Elsevier, 1975, pp. 155-160. ISBN:9780127521107

[25] E.I. Vaughan, S. Addamane, D.M. Shima, G. Balakrishnan, A.A. Hecht, High-Resistivity Semi-insulating AlSb on GaAs Substrates Grown by Molecular Beam Epitaxy, Journal of Electronic Materials, **45** (2016) 2025-2030. DOI:10.1007/s11664-016-4359-y

[26] C. Raisin, A. Rocher, G. Landa, R. Carles, L. Lassabatere, GaSb/GaAs heteroepitaxy characterized as a stress-free system, Applied Surface Science, **50** (1991) 434-439. DOI:10.1016/0169-4332(91)90213-4

[27] B.R. Bennett, W.J. Moore, M.J. Yang, B.V. Shanabrook, Transport properties of Be- and Si-doped AlSb, Journal of Applied Physics, **87** (2000) 7876-7879. DOI:10.1063/1.373470

[28] E. Selvig, Molecular beam epitaxial growth and characterization of GaInAsSb/AlGaAsSb mid-infrared laser structures, Doctoral thesis, Norwegian University of Science and Technology, Trondheim, 2004. ISBN:8247163926

[29] K.-K. Kim, S. Niki, J.-Y. Oh, J.-O. Song, T.-Y. Seong, S.-J. Park, S. Fujita, S.-W. Kim, High electron concentration and mobility in Al-doped n-ZnO epilayer achieved via dopant activation using rapid-thermal annealing, Journal of Applied Physics, **97** (2005) 066103. DOI:10.1063/1.1863416

[30] R. Bugge, B.-O. Fimland, Annealing effects in InGaAsSb quantum wells with pentenary AlInGaAsSb barriers, Physica Scripta, **T126** (2006) 15-20. `DOI:10.1088/0031-8949/2006/T126/004`

[31] Y. Wang, H. Djie, B. Ooi, Interdiffusion in InGaAsSb/ AlGaAsSb quantum wells, Journal of Applied Physics, **98** (2005) 073508. `DOI:10.1063/1.2061893`

[32] T.H. Chiu, J.A. Ditzenberger, H.S. Luftman, W.T. Tsang, N.T. Ha, Te doping study in molecular beam epitaxial growth of GaSb using Sb_2Te_3, Applied Physics Letters, **56** (1990) 1688-1690. `DOI:10.1063/1.103118`

[33] C.-C. Tin, Deep Level Transient Spectroscopy, in: Characterization of Materials, John Wiley & Sons, Inc., 2002. `ISBN:9780471266969`

[34] J. Frenkel, On pre-breakdown phenomena in insulators and electronic semi-conductors, Physical Review, **54** (1938) 647-648. `DOI:10.1103/PhysRev.54.647`

[35] M.C. Chen, D.V. Lang, W.C. Dautremont-Smith, A.M. Sergent, J.P. Harbison, Effects of leakage current on deep level transient spectroscopy, Applied Physics Letters, **44** (1984) 790-792. `DOI:10.1063/1.94887`

[36] J. Bourgoin, A. Mauger, Physical origin of the DX center, Applied Physics Letters, **53** (1988) 749-751. `DOI:10.1063/1.99821`

[37] A. Nakagawa, J.J. Pekarik, H. Kroemer, J.H. English, Deep levels in Te-doped AlSb grown by molecular beam epitaxy, Applied Physics Letters, **57** (1990) 1551-1553. `DOI:10.1063/1.103350`

[38] A. Baraldi, C. Ghezzi, A. Parisini, R. Magnanini, L. Tarricone, S. Franchi, Occupancy level of the DX center in Te-doped $Al_xGa_{1-x}Sb$, Journal of Applied Physics, **85** (1999) 256-263. `DOI:10.1063/1.369438`